Tilapia lake virus causes mitochondrial damage: a proposed mechanism that leads to extensive death in fish cells

Promporn Raksaseri [1], **Tuchakorn Lertwanakarn** [2], **Puntanat Tattiyapong** [3], **Anusak Kijtawornrat** [4], **Wuthichai Klomkleaw** [1], **Win Surachetpong** [Corresp. 3]

[1] Department of Anatomy, Faculty of Veterinary Science, Chulalongkorn University, Bangkok, Thailand

[2] Department of Physiology, Faculty of Veterinary Medicine, Faculty of Veterinary Medicine, Kasetsart University, Bangkok, Thailand

[3] Department of Veterinary Microbiology and Immunology, Faculty of Veterinary Medicine, Kasetsart University, Bangkok, Thailand

[4] Department of Physiology, Faculty of Veterinary Science, Chulalongkorn University, Bangkok, Thailand

Corresponding Author: Win Surachetpong
Email address: fvetwsp@ku.ac.th

Background. Tilapia Lake virus (TiLV), also known as *Tilapinevirus tilapiae*, poses a significant threat to tilapia aquaculture, causing extensive mortality and economic losses. Understanding the mechanisms and pathogenesis of TiLV is crucial to mitigate its impact on this valuable fish species. **Methodology.** In this study, we utilized Transmission Electron Microscopy to investigate the ultrastructural changes in E-11 cells following TiLV infection. We also examined the presence of TiLV particles within the cells. Cellular viability and mitochondrial functions were assessed using MTT and ATP measurement assays and mitochondrial probes including JC-1 staining and MitoTracker™ Red. **Results.** Our findings provide novel evidence demonstrating that TiLV causes cytotoxicity through the destruction of mitochondria. Transmission electron micrographs showed that TiLV particles were present in the cytoplasm of E-11 cells as early as 1 h after infection. Progressive swelling of mitochondria and ultrastructural damage to the cells were observed at 1, 3 and 6 days post-infection. Furthermore, losses of mitochondrial mass and membrane potential (MMP) were detected at 1 day after TiLV inoculation, as determined by mitochondrial probes. The results of the MTT assay also supported the hypothesis that the cell deaths in E-11 cells during TiLV infection may be caused by the disruption of mitochondrial structure and function. **Conclusions.** Our study reveals the significant role of mitochondrial disruption in contributing to cellular death during the early stages of TiLV infection . These findings advance the understanding of TiLV pathogenesis and further enhance our knowledge of viral diseases in fish.

Tilapia lake virus causes mitochondrial damage: a proposed mechanism that leads to extensive death in fish cells

Promporn Raksaseri[1], Tuchakorn Lertwanakarn [2], Puntanat Tattiyapong [3], Anusak Kijtawornrat [4], Wuthichai Klomkleaw[1], Win Surachetpong[3]*

[1]Department of Anatomy, Faculty of Veterinary Science, Chulalongkorn University, Bangkok, 10330, Thailand

[2]Department of Physiology, Faculty of Veterinary Medicine, Kasetsart University, Bangkok 10900, Thailand

[3]Department of Veterinary Microbiology and Immunology, Faculty of Veterinary Medicine, Kasetsart University, Bangkok 10900, Thailand

[4]Department of Physiology, Faculty of Veterinary Science, Chulalongkorn University, Bangkok, 10330, Thailand

Corresponding Author:

Win Surachetpong[1]

Department of Veterinary Microbiology and Immunology, Faculty of Veterinary Medicine, Kasetsart University, Bangkok 10900, Thailand

Email address: fvetwsp@ku.ac.th

Abstract

Background. Tilapia Lake virus (TiLV), also known as *Tilapinevirus tilapiae*, poses a significant threat to tilapia aquaculture, causing extensive mortality and economic losses. Understanding the mechanisms and pathogenesis of TiLV is crucial to mitigate its impact on this valuable fish species.

Methodology. In this study, we utilized Transmission Electron Microscopy to investigate the ultrastructural changes in E-11 cells following TiLV infection. We also examined the presence of TiLV particles within the cells. Cellular viability and mitochondrial functions were assessed using MTT and ATP measurement assays and mitochondrial probes including JC-1 staining and MitoTracker™ Red.

Results. Our findings provide novel evidence demonstrating that TiLV causes cytotoxicity through the destruction of mitochondria. Transmission electron micrographs showed that TiLV particles were present in the cytoplasm of E-11 cells as early as 1 h after infection. Progressive swelling of mitochondria and ultrastructural damage to the cells were observed at 1, 3 and 6 days post-infection. Furthermore, losses of mitochondrial mass and membrane potential (MMP) were detected at 1 day after TiLV inoculation, as determined by mitochondrial probes. The results of the MTT assay also supported the hypothesis that the cell deaths in E-11 cells during TiLV infection may be caused by the disruption of mitochondrial structure and function.

Conclusions. Our study reveals the significant role of mitochondrial disruption in contributing to cellular death during the early stages of TiLV infection. These findings advance the understanding of TiLV pathogenesis and further enhance our knowledge of viral diseases in fish.

Keywords: Tilapia Lake virus (TiLV); Tilapia; Transmission Electron Microscopy (TEM); Mitochondria; Cytotoxicity

Introduction

Tilapia lake virus disease (TiLVD) is an emerging disease caused by tilapia lake virus (TiLV) that currently affects global tilapia aquaculture (Eyngor et al. 2014; Surachetpong et al. 2020). TiLV was first described in tilapia from the Sea of Galilee, Israel in 2014, and concurrently, another virus causing high mortality and syncytial hepatitis of juvenile tilapia (SHT) was described in Ecuador (Ferguson et al. 2014). Subsequent studies have shown that SHT and TiLV share 98–100% genetic sequence identity (Del-pozo et al. 2017), and are therefore the same virus causing disease in tilapia (Bacharach et al. 2016; Ferguson et al. 2014). TiLV, also known as *Tilapinevirus tilapiae*, is classified as a member of the family *Amnoonviridae* (ICTV 2021; Sunarto et al. 2022). The virus has a spherical shape with a trilaminar capsid-like structure (Del-Pozo et al. 2017).

TiLV primarily infects tilapia and its hybrid species (Surachetpong et al. 2020; Waiyamitra et al. 2021); however, other cichlid fishes including Giant gourami (*Osphronemus goramy*) (Jaemwimol et al. 2018), ornamental African cichlids (*Aulonocara* sp.) (Yamkasem et al. 2021), and angel fish (*Pterophyllum scalare*) (Paria et al. 2023) have been found to be susceptible to TiLV infection. Clinical signs of TiLV infection include erratic swimming, skin hemorrhage, exophthalmos, abdominal swelling, anemia, and scale protrusion (Eyngor et al. 2014; Ferguson et al. 2014; Tattiyapong et al. 2017; Turner et al., 2023). Microscopic examination of infected tilapia has revealed inflammation and necrosis of various organs, including liver, spleen, head kidney, gills, and brain tissues (Mugimba et al. 2018; Pierezan et al. 2020; Tattiyapong et al. 2017). However, the mechanism behind cell death caused by TiLV infection is currently not fully understood.

Previous studies have demonstrated that TiLV can multiply and lead to cell death in various fish cell lines (Eyngor et al. 2014; Lertwanakarn et al. 2021; Li et al. 2022a; Thangaraj et al. 2018;

Wang et al. 2018; Yadav et al. 2021). A recent study by Lertwanakarn et al., 2021 revealed that TiLV infection caused cytopathic effect (CPE) in E-11 cells within 3 days, while CPE formation in other cell lines may vary between 3 to 11 days post-infection (dpi) (Li et al. 2022a; Thangaraj et al. 2018; Wang et al. 2018; Yadav et al. 2021). Transmission electron microscopy (TEM) has revealed that TiLV particles are rounded in shape and approximately 60–110 nm in size (Eyngor et al. 2014; Li et al. 2022a; Piewbang et al. 2022; Thangaraj et al. 2018; Wang et al. 2018). These particles can be found in susceptible cells as early as 3 dpi (Piewbang et al. 2022). Additionally, ultrastructural changes, such as swollen Golgi apparatus and mitochondria, as well as dense chromatin nuclei have been observed in TiLV-infected cells (Del-Pozo et al. 2017; Ferguson et al. 2014). However, the dynamic studies of TiLV on mitochondrial structure and functions have never been investigated.

Mitochondria play a crucial role in energy metabolism and the oxidative stress response in cells. In fish, mitochondria are responsible for oxygen consumption, as evident from the presence of mitochondrial-rich cells in the gills of most teleosts (Hui-Chen Lin & Wen-Ting Sung 2003). Furthermore, mitochondria are involved in apoptosis, a process of cell death. The cold stress response in Nile tilapia has been associated with reduced mitochondrial membrane potential (MMP) and ATP production, leading to cellular apoptosis in various organs (Liu et al. 2022). Additionally, pendimethalin toxicity has been shown to cause mitochondrial defects in tilapia due to excessive oxidative stress, leading to damage in the brain, spleen, and gills (Nassar et al. 2021). Similar to TiLV, infection with other piscine viruses such as the infectious spleen and kidney necrosis virus (ISKNV) in the grouper cell line GF-1 can also lead to a deterioration in mitochondrial membrane potential (MMP), increased oxidative stress, and cell apoptosis and tissue damage (Chen et al. 2022). Importantly, the disruption of mitochondrial function is one of the key

mechanisms that can lead to cell apoptosis and organ failure during viral infection and chemical toxicity. Despite its widespread distribution, there is a limited understanding of the biology and host cell alteration caused by TiLV infection. However, understanding the mechanism by which TiLV causes cell damage and changes in cellular functions can provide insights into the pathogenesis of this important virus, particularly its impact on mitochondria. Furthermore, this knowledge can be used to develop strategies to prevent and manage TiLV infections in fish populations.

In this study, we investigated the pathogenesis of TiLV infection involving the mitochondrial disruption in fish cells using TEM, cellular viability assays, and mitochondrial probes. Our findings suggest that TiLV infection leads to mitochondrial damage, impairs MMP, and induces cytotoxicity.

Materials and Methods

Propagation of TiLV

The TiLV strain VETKU-TV01, previously isolated from the brain of infected red tilapia (*Oreochromis sp.*) (Tattiyapong et al. 2017), was used in the study. E-11 cells, a clone of SSN-1 cells isolated from snakehead fish (*Ophicephalus striatus*) (Iwamoto et al. 2000) were obtained from the European Collection of Authenticated Cell Cultures (ECACC), England (catalog number 01110916). E-11 cells were cultured in Leibovitz L-15 medium supplemented with 5% fetal bovine serum (Sigma, USA) and 2 mM L-glutamine at 25°C in a CO_2-free environment until they reached 70–80% confluence. The culture medium was subsequently removed, and inoculated with a viral load of 0.1 MOI for 1 h at 25°C. Following incubation, the virus suspension and culture medium were aspirated, and the cells were thoroughly rinsed. Cells were maintained in Leibovitz

L-15 supplemented with 2% fetal bovine serum (Sigma, USA) and 2 mM L-glutamine at 25°C in a CO_2-free environment. Daily microscopic observations were conducted until 80% of the cells exhibited CPE. The protocol for handling the virus was approved by the Institutional Biosafety Committee (IBC), Faculty of Veterinary Medicine, Kasetsart University under the protocol number IBC-63-V02.

Virus purification by glucose gradient centrifugation

Once 80−100% CPE formation was observed, infected E-11 cells were disrupted using three rounds of freeze-thaw cycles followed by centrifugation at 3000 × g for 10 min. The supernatant containing TiLV was collected and stored at −80°C until further use. The supernatant was thawed and re-suspended in a 30% sucrose solution in 14 x 89 mm thin wall polypropylene centrifuge tubes (Beckman Coulter, USA). The suspension was then centrifuged at 40,000 rpm (10000 × g) for 1.5 h at 4°C using an Optima L-90K Ultracentrifuge (Beckman Coulter, USA). The pellet was collected and resuspended in 1 mL of TN buffer (0.1 M NaCl, 0.01 M Tris pH 7.4). The suspension was overlaid on top of a glucose gradient solution consisting of 2 mL layers of 30%, 40%, and 50% (w/v) sucrose in TNE buffer (0.1 M NaCl, 0.01 M Tris pH 7.4, 3 mM EDTA) and subjected to centrifugation at 40,000 rpm for 1.5 h at 4°C. Two mL of each fraction was collected and mixed with 10 mL of phosphate buffer saline (PBS) buffer. To remove excess sucrose solution, the suspension was ultracentrifuged at 40,000 rpm for 30 min at 4°C. The supernatant was discarded, and 500 µL of PBS solution was added to each fraction, which was then stored at 4°C until further analysis.

134 Transmission electron microscopy (TEM) with positive staining

135 Uninfected and infected E-11 cells were collected at 0, 1, 3, and 6 dpi. Cells were
136 trypsinized from the culture flasks and transferred to a 1.5 mL tube at room temperature (25°C).
137 The cell suspension was centrifuged at 2,000 rpm for 5 min at 4°C (Centrifuge 5418R, Eppendorf,
138 Germany). The supernatant was discarded, and the pellet was resuspended in 500 µL of 0.1 M
139 PBS, followed by incubation in 2.5% glutaraldehyde in 0.1 M PBS at 4°C overnight. The following
140 day, the samples were thoroughly rinsed with 0.1 M PBS for 10 min, three times. The cell pellets
141 were then incubated with 1% osmium tetroxide in dH_2O for 1 h according to a previous protocol
142 (Barreto-Vieira and Barth, 2015). The pellets were rinsed with dH_2O for 10 min three times,
143 dehydrated in acetone, and embedded in resin. Ultrathin sections were prepared by cutting samples
144 at 90 nm thick using a glass knife. Samples were placed on a thin copper grid for 15 min and
145 stained with 5% uranyl acetate for 15 min and lead citrate for 15 min. Samples were examined
146 under a Hitachi HT7700 transmission electron microscope (Hitachi, Germany) at the Scientific
147 Equipment and Research Division, Kasetsart University, Bangkok, Thailand. All micrographs
148 were taken at 80 kV.
149
150 Transmission electron microscopy (TEM) with negative staining
151 The purified TiLV was suspended in PBS (4°C) and then transferred to Formvar® film-
152 coated copper grids with 400 mesh sizes (Electron Microscopy Science, USA) for 30 min. The
153 grids were washed with dH_2O before being stained with 40 µL of 2% uranyl acetate or 1%
154 phosphotungstic acid for 1 min using filtered paper to remove the staining solution. The samples
155 were dried for 7 days and then observed with the TEM operating at 80 kV.
156

Cell Viability Assay

The cell viability was determined by 3-[4,5-dimethylthiazol-2-yl]-2,5-diphenyl tetrazolium bromide (MTT) assay. Briefly, E-11 cells were seeded in a 96-well plate at a density of $4x10^4$ cells/mL per well and incubated overnight with L-15 medium supplemented with 5% FBS at 25°C without CO_2. The cells were then infected with TiLV at 0.1 MOI for 1 h in a humidified incubator at 25°C. Next, cells were incubated with MTT at a concentration of 5 mg/mL in L-15 media for 4 h in a 37°C humidified incubator. The uninfected and infected E-11 cells were collected at 1 h (0 days), 1, 3, and 6 days after TiLV inoculation and used as control and experimental groups, respectively. The media containing MTT were then removed and replaced with 100% DMSO to solubilize formazan, and the absorbance of the solubilized formazan in each group was measured using a hybrid multi-mode microplate reader (Synergy™ H1, Agilent, USA) at a wavelength of 590 nm.

Measurement of ATP concentration

The ATP concentration of the cells was evaluated using the CellTiter-Glo® luminescent cell viability assay (Promega, Madison, WI, USA). E-11 cells were incubated at 25°C, 100% O_2 overnight. The cells were then treated with TiLV at 0.1 MOI (n=3) for one hour before being replaced with Leibovitz's medium containing 2 fetal bovine serum (2% FBS L-15). Cells treated with 2% FBS L-15 and blank were included as negative controls. The measurement of ATP concentration was performed on 0, 1, 3, and 6 dpi, by extrapolating from the ATP (Sigma, St Louis, MO, USA) standard curve (10−1,000 nM). Luminescence was detected using a luminometer (Synergy H1™, BioTek® Instruments, Inc., Winooski, VT, USA) for 1 s at 37°C, and

179 the relative light units were read using Gen5™ software (BioTek® Instruments, Inc., Winooski,
180 VT, USA).
181
182 ## Detection of red-to-green ratio in JC-1-stained E-11 cells
183 The mitochondrial function of E-11 was evaluated using the fluorochrome 5,5′,6,6′-
184 tetrachloro-1,1′,3,3′ tetraethylbenzimidazolyl-carbocyanine iodide (JC-1) (Molecular probes Inc,
185 USA). E-11 cells were plated in 24-well flat-bottom plates and allowed to reach 70−100%
186 confluence. The cells were then infected with 0.1 MOI of TiLV for 1 h, followed by the
187 replacement of 2% FBS L-15, and further incubation at 25°C. Uninfected E-11 cells were used as
188 a control. At 0, 1, 3, and 6 dpi, the cells were incubated with 5 μM of JC-1 for 30 min, washed
189 with PBS twice, and visualized under an inverted fluorescence microscope (IX73, Olympus,
190 Japan). Green and red images were captured and analyzed under the BW channel (bandpass
191 460−495 nm; barrier filter 510 nm; dichroic mirror 505 nm) and GW channel (bandpass 530−550
192 nm; barrier filter 575 nm; dichroic mirror 570 nm), respectively. All pictures were merged into a
193 new image using cellSens dimension™ 2.3 software (Olympus, Japan). The intensity of green and
194 red colors was randomly analyzed from three dispersed areas with more than 1,000,000 pixels, and
195 the average red-to-green (R/G) ratios were calculated and compared between uninfected and
196 TiLV-infected E-11 cells.
197
198 ## Determination of mitochondrial mass in E-11 cells
199 The number of mitochondria was investigated using MitoTracker™ Red CMXRos staining
200 (Invitrogen™, Eugene, OR, USA). The E-11 cell line was cultured in Leibovitz's L-15 media with
201 5% FBS at 25°C without CO_2. After trypsinization and cell counting, the cells were seeded onto

collagen-coated cover slips and allowed to incubate until they reached 80–90% confluence. Subsequently, the cells were inoculated with TiLV at 0.1 MOI and then stained with MitoTracker™ in a dark room. Following staining, the cells were fixed with methanol and permeabilized using Triton X-100 (Sigma, St Louis, MO, USA). To visualize the cell nuclei, the cells were further incubated with 4',6-diamidino-2-phylindole (DAPI) at a concentration of 1:1,000. Representative images were acquired using confocal laser scanning microscope model FLUOVIEW FV3000 (Olympus, Tokyo, Japan) with specific filters for MitoTracker™ Red (579 nm excitation/599 nm emission), and DAPI (358 nm excitation/461 nm emission).

Statistical analysis

All data were statistically analyzed using GraphPad™ Prism software (San Diego, CA, USA). Results were shown as the mean ± standard error of the mean (S.E.M.). The data were tested for normal distribution using Kolgomorov-Smirnov test, and all data followed a Gaussian distribution. The cell viability, ATP measurement and JC-1 red-to-green ratios were compared between uninfected and TiLV-infected at 0, 1, 3, and 6 dpi using two-way ANOVA, followed by Tukey's as a post-hoc test. Statistical significance was considered at p-value less than 0.05.

Results

TiLV caused morphological changes and cytopathic effects in E-11 cells.

The infection of E-11 cells with TiLV resulted in significant morphological changes and cytopathic effects (CPE). Within 24 h of infection, the infected cells showed altered morphology, with CPE progression from 10% to 90% between 1 to 6 days post-infection (dpi). At 1 dpi, uninfected cells remained normal (as seen in Fig. 1A), while infected cells exhibited vacuolation

and pyknotic nuclei (as seen in Fig. 1B). By 3 dpi (as seen in Fig. 1C) and 6 dpi (as seen in Fig. 1D), extensive vacuolation, shrinkage, and distinct CPE formation were observed, with only a limited number of viable cells remaining and discoloration of the culture media at 6 dpi. These findings demonstrate that TiLV infection leads to substantial changes in the morphology and viability of E-11 cells.

Ultrastructural changes of E-11 cells during TiLV infection

The ultrastructure of uninfected and TiLV-infected E-11 cells was compared using TEM. Figure 2A and 2C depict the ultrastructure of uninfected cells, while Figure 2B and 2D demonstrate the ultrastructure of TiLV-infected cells. Within 1 h post-infection (0 dpi), a viral particle was observed at the plasma membrane of the infected E-11 cells (Fig. 2B; inset). However, no significant changes in the cellular structure and organelles were noticed at this early time point. Both uninfected and TiLV-infected cells exhibited intact nuclear membranes, normal mitochondria (Fig. 2C and 2D), and typical rough endoplasmic reticulum (rER) at 0 dpi (Fig. 2A, 2B, and 2C).

At 1 dpi, the uninfected cell displayed both normal mitochondria and mitochondria with partial loss of cristae (Fig. 3A). In contrast, TiLV-infected cells exhibited initial changes, including swollen mitochondria, indistinct mitochondrial membrane structure, and cristae degeneration (Fig. 3B). At 3 dpi, cristae remained visible in the mitochondria of uninfected cells (Fig. 3C), while progressive mitochondrial degeneration was observed in TiLV-infected cells, characterized by extensive cristae loss. Furthermore, TiLV-infected cells displayed the formation of lamellar bodies and a large number of free TiLV particles (Fig. 3D). At 6 dpi, uninfected cells still maintained intact mitochondrial membranes and cristae (Fig. 3E). In contrast, TiLV-infected cells exhibited

multiple cytoplasmic vacuolations. At this time point, the mitochondria showed progressive degeneration, including swelling, major structural distortion, delamination of the inner and outer mitochondrial membranes, and complete loss of cristae. Intracytoplasmic TiLV particles were also prominently present (Fig. 3F). Additionally, the ultrastructure of isolated TiLV particles was examined in Supplementary Figure 1. The particles were found to have a round or oval shape, with diameters ranging from 50 to 120 nm. The particles exhibited a central electron-dense core surrounded by a capsid-like bilaminar structure. Notably, the spike protein was not observed on the surface of the TiLV particles.

TiLV caused extensive mitochondrial damage and cell death.

To evaluate the impact of TiLV infection on cellular viability and mitochondrial damage in E-11 cells, the MTT assay, ATP measurement, and JC-1 staining were employed (Fig. 4). The MTT assay revealed that TiLV infection resulted in significant cell death, with a progressive decline in the number of viable cells from 104.39±5.85% at 0 dpi to 6.89±7.21% at 6 dpi (Fig. 4A). Likewise, the amount of ATP concentration in E-11 cells following TiLV infection gradually reduced from 1.01±0.01 µM at 0 dpi to 0.77±0.03 µM at 6 dpi (Fig. 4B). Notably, the JC-1 staining demonstrates the alteration of mitochondrial membrane potential as indicated by red-to-green fluorescence (R/G) ratio in TiLV-infected cells (Fig. 4C & 4D). At 0 dpi, there was no significant difference in the R/G ratio (1.22±0.06) in TiLV-infected cells compared to uninfected cells (1.50±0.05). However, at 1 dpi, the R/G ratio decreased to 1.03±0.06 and remained at a similar level at 3 dpi (1.012±0.04) and 6 dpi (1.00±0.11). Additionally, the MitoTracker™ Red staining revealed loss of mitochondrial mass following TiLV infection at 1 dpi (Fig. 5). Comparison of the MTT assay, ATP measurement and JC-1 staining between control and TiLV-infected cells revealed statistical significance at 1, 3, and 6 dpi ($p<0.05$). These results indicated significant

damage to the mitochondria and reduction in cellular viability in E-11 cells following TiLV infection.

Discussion

TiLV is a globally significant pathogen in tilapia aquaculture, causing substantial mortality and economic losses in over 18 countries (Eyngor et al. 2014; He et al. 2023; Surachetpong et al. 2020; Tran et al. 2022). While research in this area has primarily focused on epidemiology, susceptible fish species, diagnosis, and vaccine development, the underlying mechanisms by which the virus induces cell death remain poorly understood. This study provides insights into the subcellular damage of mitochondria caused by TiLV infection, which results in a decrease in MMP, mitochondrial mass, ATP production and cell viability as indicated by mitochondrial probes and cellular viability assays. These findings suggest that mitochondrial structural and functional deterioration may be a key mechanism contributing to cell death during TiLV infection.

Previous research have demonstrated the susceptibility of various cell lines to TiLV infection, including E-11 cells, a cloned cell line derived from striped snakehead (*Channa striatus*, SSN-1) cell line (Iwamoto et al. 2000; Lertwanakarn et al. 2021), and primary tilapia (*Oreochromis* spp.) cell lines isolated from the brain, heart, and liver (Eyngor et al. 2014; Li et al. 2022a; Li et al. 2022b; Yadav et al. 2021). Furthermore, TiLV has been shown to infect primary cells from Mozambique tilapia (*O. mossambicus*) (Kembou Tsofack et al. 2017; Nanthini et al. 2019) as well as other fish cells (Li et al. 2022a). Despite this knowledge, the cellular damage mechanisms and physiological changes in fish cells during TiLV infection have not been extensively studied.

In this study, TEM was employed to investigate the ultrastructural changes of E-11 cells upon TiLV infection. Interestingly, intracellular viral particles were observed within one hour of

infection as previously reported in endothelial cells derived from the heart (*bulbus arteriosus*) tissue of tilapia (Abu Rass et al. 2022). The size and shape of TiLV were also consistent with previous descriptions, appearing as round to oval structures with a diameter of 50 – 120 nm and lacking a spike protein (Del-Pozo et al. 2017; Eyngor et al. 2014; Tattiyapong et al. 2017; Yadav et al. 2021). Similarly, TEM studies revealed the presence of TiLV particles in the liver of infected fish, in both laboratory and natural settings, although the specific mechanism of cell entry remains undetermined (Del-Pozo et al. 2017; Tattiyapong et al. 2017). Recent reports demonstrated that TiLV enters tilapia cells via a cholesterol-dependent, dynamin-mediated endocytosis mechanism (Abu Rass et al. 2022) and MAPK-dependent signaling pathway (Lertwanakarn et al., 2023). In our study, we observed notable changes in the intracellular structure and organelles of infected E-11 cells within 1 dpi. Initial changes could be observed in mitochondria including mitochondrial distortion, swelling, and loss of cristae. With further progression of the infection, the appearance of lamella bodies, as along with rapid organelle damages and cell death was found between 3 to 6 days post-infection. Our results are consistent with previous studies by Del-Pozo et al. (2017) and Ferguson et al. (2014), which reported cellular and organelle damage in the hepatocytes of naturally infected fish, including an enlarged Golgi apparatus and swollen mitochondria with loss of cristae.

From our perspective, further research using other cell lines would be beneficial to replicate the findings of this study, which demonstrated that TiLV infection leads to significant damage to mitochondria, loss of its function and a decline in cellular viability. Mitochondria, as a crucial component of cellular energy production, have been found to be targeted by various viruses in both fish and mammals (Chen et al. 2022; Elesela & Lukacs 2021; Singh et al. 2020; Wang et al. 2020). For instance, the SARS-CoV-2 virus, responsible for COVID-19, targets mitochondria and

317 induces depolarization of the mitochondrial membrane potential, leading to the release of reactive
318 oxygen species and greater virulence (Shang et al. 2022). Likewise, the hepatitis E virus targets
319 gerbil brain tissue and causes mitochondrial damage, resulting in the disappearance of cristae and
320 matrix (Tian et al. 2019). In fish, the Infectious Spleen and Kidney Necrosis Virus (ISKNV)
321 disrupts the MMP by promoting the generation of pro-apoptotic Bax and Bak proteins and
322 inhibiting anti-apoptotic Bcl-2 protein, leading to cell apoptosis and necrosis (Chen et al., 2022).
323 Our study provides the first evidence on the role of mitochondrial damage in the
324 pathogenesis of cellular death during TiLV infection. The disruption of mitochondrial function
325 was demonstrated through various assays, including ATP measurement, and the application of
326 mitochondrial probes such as JC-1 and MitoTracker™ staining. Indeed, JC-1 and MitoTracker™
327 red are widely accepted and reliable methods for assessing changes in MMP and mitochondrial
328 mass. Specifically, it was found that alterations in MMP occurred within 1 day after TiLV
329 infection, which coincided with a reduction in the number of viable cells within the same
330 timeframe. Additionally, a decrease in mitochondrial mass was evident in the TiLV-infected cells
331 within 1 day, and intracellular ATP levels decreased significantly within 3 days, followed by a
332 substantial increase in cell death. This finding is consistent with a previous report showing that the
333 fish herpesvirus protein (CaHV-138L) binds to the mitochondrial FoF1-ATPase and disrupt its
334 function (Zhao et al. 2020). Notably, our preliminary inquiries conducted through the MitoFates
335 database (http://mitf.cbrc.jp/MitoFates) identify the potential involvement of a hypothetical
336 protein located within segment 6 of TiLV in mitochondrial interactions. In influenza A virus, it
337 has been demonstrated that PB1-F2 protein promotes apoptosis in infected cells by interacting to
338 two mitochondrial proteins, adenine nucleotide translocator 3 (ANT3) and voltage-dependent
339 anion channel 1 (VDAC1). This interaction leads to the compromise of mitochondrial integrity

and the subsequent cytochrome C release (Zamarin et al. 2005). Nevertheless, the mechanisms underlying mitochondrial damage, along with the specific proteins associated with TiLV and mitochondria require further in-depth investigation. Collectively, these findings highlight the crucial role of mitochondria during viral infections and emphasize the potential role of viruses to target and impair the cellular organelle.

Our novel findings align with earlier studies that have shown that mitochondria are frequently targeted by fish viruses and play a vital role in the pathogenesis and cell death process (Chen et al. 2022). While this study did not provide conclusive evidence that TiLV specifically invades or attaches to mitochondrial proteins, TEM revealed that viral particles were located close to the organelle and caused substantial damage during infection. Further research is necessary to fully comprehend the mechanisms by which TiLV damages mitochondria such as oxygen consumption rate, and investigation of specific signaling pathways, genes, and proteins involved in the process.

Conclusions

In summary, our study provides evidence of the virulence and pathogenesis of TiLV, through the detection of viral particles in infected cells, the damage of mitochondria, reduction in ATP production, mitochondria mass, and cell death. Understanding the connections between mitochondrial damage and physiological disturbance in tilapia hosts, while considering other environmental factors that contribute to virus transmission, such as water quality, virus shedding, and genetic variation between viruses and hosts, is crucial for comprehending the impact of virus-host interactions on disease transmission and the fitness of TiLV in tilapia. Further research on the

pathogenic mechanisms of TiLV in fish *in vivo* will expand our understanding of the virus-fish interaction.

Figure legends

Figure 1 Morphological changes and cytopathic effects of TiLV infection in E-11 cells. (A) Uninfected E-11 cells showing a normal appearance and confluence (B) TiLV-infected E-11 cells at 1 dpi displaying vacuolation (arrow) and pyknotic nuclei (arrowhead) (C) TiLV-infected E-11 cells at 3 dpi exhibiting extensive cell vacuolation, cell shrinkage, and cytopathic effects (CPE; asterisks). (D) TiLV-infected E-11 cells at 6 dpi showing complete cell detachment and CPE formation.

Figure 2 Representative TEM micrographs of uninfected and TiLV-infected E-11 cells at 0 dpi (1 h post-TiLV inoculation). (A) Uninfected E-11 cell with normal mitochondria (arrows), and nucleus (N). (B) TiLV-infected E-11 cell with normal nucleus (N), rough endoplasmic reticulum (rER: arrowhead), and presence of intracytoplasmic TiLV particle close to the plasma membrane (inset). (C) Uninfected E-11 cell under higher magnification showing normal mitochondria (arrow) and rER (arrowheads). (D) TiLV-infected E-11 cells under higher magnification showing normal mitochondria (arrow).

Figure 3 Time course of ultrastructural changes in TiLV-infected compared to uninfected E-11 cells. (A) Uninfected cell at 1 dpi presenting a normal mitochondrion with intact cristae (white arrow) and mitochondria with partial loss of cristae (black arrows). (B) TiLV-infected cell at 1

385 dpi, moderate mitochondrial damage (arrowhead) with the presence of a TiLV particle close to the
386 plasma membrane (arrow). Nuclear membrane is still intact (asterisk). (C) Uninfected cell at 3 dpi
387 displaying normal mitochondria and some mitochondria with partial loss of cristae (arrowhead),
388 N = nucleus. (D) TiLV-infected cell at 3 dpi, a mitochondrion without cristae (arrowhead), and
389 abundance of TiLV particles (arrow) close to lamellar bodies (asterisk) can be seen. (E) Uninfected
390 cell with normal mitochondrion (arrowhead) near the intact nuclear membrane (asterisk), N=
391 nucleus. (F) TiLV-infected cell at 6 dpi presenting a group of extensive degenerated mitochondria
392 (arrowheads) surrounding TiLV particles (arrow), N = nucleus.
393
394 **Figure 4** Determination of mitochondrial structural and functional damage upon TiLV-infected E-
395 11 cells at 0, 1, 3, and 6 dpi. (A) Survival of E-11 cells after TiLV infection assessed by MTT
396 assay. (B) ATP concentration measured using CellTiter-Glo® assay (C) Mitochondrial damage in
397 TiLV-infected cells was analyzed based on the red-to-green ratio of JC-1-stained E-11 cells. Data
398 were quantified from three separate fields of overlay picture and shown as average values. All data
399 were represented as the mean ± standard error of mean (S.E.M.) from three independent
400 experiments. (D) Bright field (BF), red cells (JC-1 aggregate), green cells (JC-1 monomer), and
401 overlay pictures of uninfected and TiLV-infected E-11 cells. Statistical significance between
402 uninfected and TiLV-infected cells is denoted by *p<0.05, **p<0.01, and ***p<0.001.
403
404 **Figure 5** Representative images of E-11 at 1 dpi incubated with MitoTracker™ Red staining (A)
405 Uninfected cells (B) TiLV-infected cells. The nuclei were stained with DAPI.
406

Supplementary Figure 1. Negative staining of a TiLV particle under the transmission electron microscope exhibiting a round to oval shape at 50−120 nm with a central electron-dense core, surrounded by a capsid-like bilaminar structure.

References

Abu Rass R, Kembou-Ringert JE, Zamostiano R, Eldar A, Ehrlich M, and Bacharach E. 2022. Mapping of Tilapia Lake Virus entry pathways with inhibitors reveals dependence on dynamin activity and cholesterol but not endosomal acidification. *Front Cell Dev Biol* 10:1075364. 10.3389/fcell.2022.1075364

Bacharach E, Mishra N, Briese T, Zody MC, Kembou Tsofack JE, Zamostiano R, Berkowitz A, Ng J, Nitido A, Corvelo A, Toussaint NC, Abel Nielsen SC, Hornig M, Del Pozo J, Bloom T, Ferguson H, Eldar A, and Lipkin WI. 2016. Characterization of a Novel Orthomyxo-like Virus Causing Mass Die-Offs of Tilapia. *mBio* 7:e00431-00416. 10.1128/mBio.00431-16

Chen PH, Hsueh TC, Wu JL, and Hong JR. 2022. Infectious Spleen and Kidney Necrosis Virus (ISKNV) Triggers Mitochondria-Mediated Dynamic Interaction Signals via an Imbalance of Bax/Bak over Bcl-2/Bcl-xL in Fish Cells. *Viruses* 14. 10.3390/v14050922

Del-Pozo J, Mishra N, Kabuusu R, Cheetham S, Eldar A, Bacharach E, Lipkin WI, and Ferguson HW. 2017. Syncytial Hepatitis of Tilapia (Oreochromis niloticus L.) is Associated With Orthomyxovirus-Like Virions in Hepatocytes. *Vet Pathol* 54:164-170. 10.1177/0300985816658100

Elesela S, and Lukacs NW. 2021. Role of Mitochondria in Viral Infections. *Life* 11:232.

Eyngor M, Zamostiano R, Kembou Tsofack JE, Berkowitz A, Bercovier H, Tinman S, Lev M, Hurvitz A, Galeotti M, Bacharach E, and Eldar A. 2014. Identification of a novel RNA virus lethal to tilapia. *J Clin Microbiol* 52:4137-4146. 10.1128/jcm.00827-14

Ferguson HW, Kabuusu R, Beltran S, Reyes E, Lince JA, and del Pozo J. 2014. Syncytial hepatitis of farmed tilapia, Oreochromis niloticus (L.): a case report. *J Fish Dis* 37:583-589. 10.1111/jfd.12142

He T, Zhang Y-Z, Gao L-H, Miao B, Zheng J-S, Pu D-C, Zhang Q-Q, Zeng W-W, Wang D-S, Su S-Q, and Zhu S. 2023. Identification and pathogenetic study of tilapia lake virus (TiLV) isolated from naturally diseased tilapia. *Aquaculture* 565:739166. https://doi.org/10.1016/j.aquaculture.2022.739166

Hui-Chen Lin, and Wen-Ting Sung. 2003. The Distribution of Mitochondria-Rich Cells in the Gills of Air-Breathing Fishes. *Physiological and Biochemical Zoology* 76:215-228. 10.1086/374278

ICTV. 2021. Virus Taxonomy: 2021 Release.

Iwamoto T, Nakai T, Mori K, Arimoto M, and Furusawa I. 2000. Cloning of the fish cell line SSN-1 for piscine nodaviruses. *Dis Aquat Organ* 43:81-89. 10.3354/dao043081

Jaemwimol P, Rawiwan P, Tattiyapong P, Saengnual P, Kamlangdee A, and Surachetpong W. 2018. Susceptibility of important warm water fish species to tilapia lake virus (TiLV) infection. *Aquaculture* 497:462-468. https://doi.org/10.1016/j.aquaculture.2018.08.028

Kembou Tsofack JE, Zamostiano R, Watted S, Berkowitz A, Rosenbluth E, Mishra N, Briese T, Lipkin WI, Kabuusu RM, Ferguson H, Del Pozo J, Eldar A, and Bacharach E. 2017. Detection of Tilapia Lake Virus in Clinical Samples by Culturing and Nested Reverse Transcription-PCR. *J Clin Microbiol* 55:759-767. 10.1128/jcm.01808-16

453 Lertwanakarn T, Trongwongsa P, Yingsakmongkol S, Khemthong M, Tattiyapong P, and
454 Surachetpong W. 2021. Antiviral Activity of Ribavirin against Tilapia tilapinevirus in Fish
455 Cells. *Pathogens* 10. 10.3390/pathogens10121616
456 Lertwanakarn T, Khemthong M, Tattiyapong P, and Surachetpong W. 2023. The Modulation of
457 Immune Responses in Tilapinevirus tilapiae-Infected Fish Cells through MAPK/ERK
458 Signalling. Viruses. 15:900. doi.org/10.3390/v15040900
459 Li B, Zheng S, Wang Y, Wang Q, Li Y, Yin J, Ren Y, Shi C, Zhao Z, Jiang Z, Bergmann SM, and
460 Zeng W. 2022a. Susceptibilities of ten fish cell lines to infection with Tilapia lake virus.
461 *Microbial Pathogenesis* 166:105510. https://doi.org/10.1016/j.micpath.2022.105510
462 Li Y, Huang Y, Cai J, Jiang D, Jian JC, Lu YS, and Wang B. 2022b. Establishment of an astrocyte-
463 like cell line from the brain of tilapia (Oreochromis niloticus) for virus pathogenesis and a
464 vitro model of the blood-brain barrier. *J Fish Dis*. 10.1111/jfd.13674
465 Liu R, Liu R, Song G, Li Q, Cui Z, and Long Y. 2022. Mitochondria Dysfunction and Cell
466 Apoptosis Limit Resistance of Nile Tilapia (Oreochromis niloticus) to Lethal Cold Stress.
467 Animals.
468 Mugimba KK, Chengula AA, Wamala S, Mwega ED, Kasanga CJ, Byarugaba DK, Mdegela RH,
469 Tal S, Bornstein B, Dishon A, Mutoloki S, David L, Evensen Ø, and Munang'andu HM.
470 2018. Detection of tilapia lake virus (TiLV) infection by PCR in farmed and wild Nile
471 tilapia (Oreochromis niloticus) from Lake Victoria. *J Fish Dis*. 10.1111/jfd.12790
472 Nanthini R, Abdul Majeed S, Vimal S, Taju G, Sivakumar S, Santhosh Kumar S, Pillai D, Sneha
473 KG, Rakesh CG, and Sahul Hameed AS. 2019. In vitro propagation of tilapia lake virus in
474 cell lines developed from Oreochromis mossambicus. *Journal of Fish Diseases* 42:1543-
475 1552. https://doi.org/10.1111/jfd.13075

476 Nassar AMK, Abdel-Halim KY, and Abbassy MA. 2021. Mitochondrial biochemical and
477 histopathological defects induced by the herbicide pendimethalin in tilapia fish
478 (Oreochromis niloticus). *Comparative Biochemistry and Physiology Part C: Toxicology &*
479 *Pharmacology* 242:108949. https://doi.org/10.1016/j.cbpc.2020.108949
480 Paria A, Yadav SC, Verma DK, Mishra A, Rastogi A, Ravindra, Swaminathan TR, Rajendran KV,
481 Sood N, and Pradhan PK. 2023. Susceptibility of selected tropical non-tilapine ornamental
482 cichlids to Tilapia tilapinevirus following experimental infection. *Aquaculture*
483 567:739224. https://doi.org/10.1016/j.aquaculture.2022.739224
484 Pierezan F, Yun S, Piewbang C, Surachetpong W, and Soto E. 2020. Pathogenesis and immune
485 response of Nile tilapia (Oreochromis niloticus) exposed to Tilapia lake virus by
486 intragastric route. *Fish & Shellfish Immunology* 107:289-300.
487 https://doi.org/10.1016/j.fsi.2020.10.019
488 Piewbang C, Tattiyapong P, Khemthong M, Lachroje S, Boonrungsiman S, Kasantikul T,
489 Surachetpong W, and Techangamsuwan S. 2022. Dual infections of tilapia parvovirus
490 (TiPV) and tilapia lake virus (TiLV) in multiple tilapia farms: Their impacts, genetic
491 diversity, viral tropism, and pathological effects. *Aquaculture* 550:737887.
492 https://doi.org/10.1016/j.aquaculture.2022.737887
493 Shang C, Liu Z, Zhu Y, Lu J, Ge C, Zhang C, Li N, Jin N, Li Y, Tian M, and Li X. 2022. SARS-
494 CoV-2 Causes Mitochondrial Dysfunction and Mitophagy Impairment. *Frontiers in*
495 *Microbiology* 12. 10.3389/fmicb.2021.780768
496 Singh KK, Chaubey G, Chen JY, and Suravajhala P. 2020. Decoding SARS-CoV-2 hijacking of
497 host mitochondria in COVID-19 pathogenesis. *American Journal of Physiology-Cell*
498 *Physiology* 319:C258-C267. 10.1152/ajpcell.00224.2020

499 Sunarto A, Grimm J, McColl KA, Ariel E, Krishnankutty Nair K, Corbeil S, Hardaker T, Tizard
500 M, Strive T, and Holmes B. 2022. Bioprospecting for biological control agents for invasive
501 tilapia in Australia. *Biological Control* 174:105020.
502 https://doi.org/10.1016/j.biocontrol.2022.105020
503 Surachetpong W, Roy SRK, and Nicholson P. 2020. Tilapia lake virus: The story so far. *Journal*
504 *of Fish Diseases* 43:1115-1132. https://doi.org/10.1111/jfd.13237
505 Tattiyapong P, Dachavichitlead W, and Surachetpong W. 2017. Experimental infection of Tilapia
506 Lake Virus (TiLV) in Nile tilapia (Oreochromis niloticus) and red tilapia (*Oreochromis*
507 spp.). *Vet Microbiol* 207:170-177. 10.1016/j.vetmic.2017.06.014
508 Thangaraj RS, Ravi C, Kumar R, Dharmaratnam A, Valaparambil Saidmuhammed B, Pradhan
509 PK, and Sood N. 2018. Derivation of two tilapia (Oreochromis niloticus) cell lines for
510 efficient propagation of Tilapia Lake Virus (TiLV). *Aquaculture* 492:206-214.
511 https://doi.org/10.1016/j.aquaculture.2018.04.012
512 Tian J, Shi R, Xiao P, Liu T, She R, Wu Q, An J, Hao W, and Soomro M. 2019. Hepatitis E Virus
513 Induces Brain Injury Probably Associated With Mitochondrial Apoptosis. *Front Cell Infect*
514 *Microbiol* 9:433. 10.3389/fcimb.2019.00433
515 Tran TH, Nguyen VTH, Bui HCN, Tran YBT, Tran HTT, Le TTT, Vu HTT, and Ngo TPH. 2022.
516 Tilapia Lake Virus (TiLV) from Vietnam is genetically distantly related to TiLV strains
517 from other countries. *J Fish Dis.* 45:1389-1401. https://doi.org/10.1111/jfd.13669
518 Turner JK, Sakulpolwat S, Sukdanon S, Lertwanakarn T, Waiyamitra P, Piewbang C, Pierezan F,
519 Techangamsuwan S, Soto E, and Surachetpong W. 2023. Tilapia lake virus (TiLV) causes
520 severe anaemia and systemic disease in tilapia. *J Fish Dis*. 46:643-651. doi:
521 10.1111/jfd.13775.

522 Waiyamitra P, Piewbang C, Techangamsuwan S, Liew WC, and Surachetpong W. 2021. Infection
523 of Tilapia tilapinevirus in Mozambique Tilapia (Oreochromis mossambicus), a Globally
524 Vulnerable Fish Species. *Viruses* 13:1104.
525 Wang P, Luo R, Zhang M, Wang Y, Song T, Tao T, Li Z, Jin L, Zheng H, Chen W, Zhao M,
526 Zheng Y, and Qin J. 2020. A cross-talk between epithelium and endothelium mediates
527 human alveolar–capillary injury during SARS-CoV-2 infection. *Cell Death & Disease*
528 11:1042. 10.1038/s41419-020-03252-9
529 Wang Y, Wang Q, Zeng W, Yin J, Li Y, Ren Y, Shi C, Bergmann SM, and Zhu X. 2018.
530 Establishment and characterization of a cell line from tilapia brain for detection of tilapia
531 lake virus. *Journal of Fish Diseases* 41:1803-1809. https://doi.org/10.1111/jfd.12889
532 Yadav MK, Rastogi A, Criollo Joaquin MP, Verma DK, Rathore G, Swaminathan TR, Paria A,
533 Pradhan PK, and Sood N. 2021. Establishment and characterization of a continuous cell
534 line from heart of Nile tilapia Oreochromis niloticus and its susceptibility to tilapia lake
535 virus. *J Virol Methods* 287:113989. 10.1016/j.jviromet.2020.113989
536 Yamkasem J, Piewbang C, Techangamsuwan S, Pierezan F, Soto E, and Surachetpong W. 2021.
537 Susceptibility of ornamental African cichlids Aulonocara spp. to experimental infection
538 with Tilapia lake virus. *Aquaculture* 542:736920.
539 https://doi.org/10.1016/j.aquaculture.2021.736920
540 Zamarin D, García-Sastre A, Xiao X, Wang R, Palese P. 2005. Influenza Virus PB1-F2 Protein
541 Induces Cell Death through Mitochondrial ANT3 and VDAC1. *PLoS Pathog* 1(1): e4.
542 https://doi.org/10.1371/journal.ppat.0010004

543 Zhao Y-H, Zeng X-T, and Zhang Q-Y. 2020. Fish herpesvirus protein (CaHV-138L) can target to
544 mitochondrial protein FoF1 ATPase. *Virus Research* 275:197754.
545 https://doi.org/10.1016/j.virusres.2019.197754

546

Figure 1

Morphological changes and cytopathic effects of TiLV infection in E-11 cells.

Figure 1 Morphological changes and cytopathic effects of TiLV infection in E-11 cells. (A) Uninfected E-11 cells showing a normal appearance and confluence (B) TiLV-infected E-11 cells at 1 dpi displaying vacuolation (arrow) and pyknotic nuclei (arrowhead) (C) TiLV-infected E-11 cells at 3 dpi exhibiting extensive cell vacuolation, cell shrinkage, and cytopathic effects (CPE; asterisks). (D) TiLV-infected E-11 cells at 6 dpi showing complete cell detachment and CPE formation.

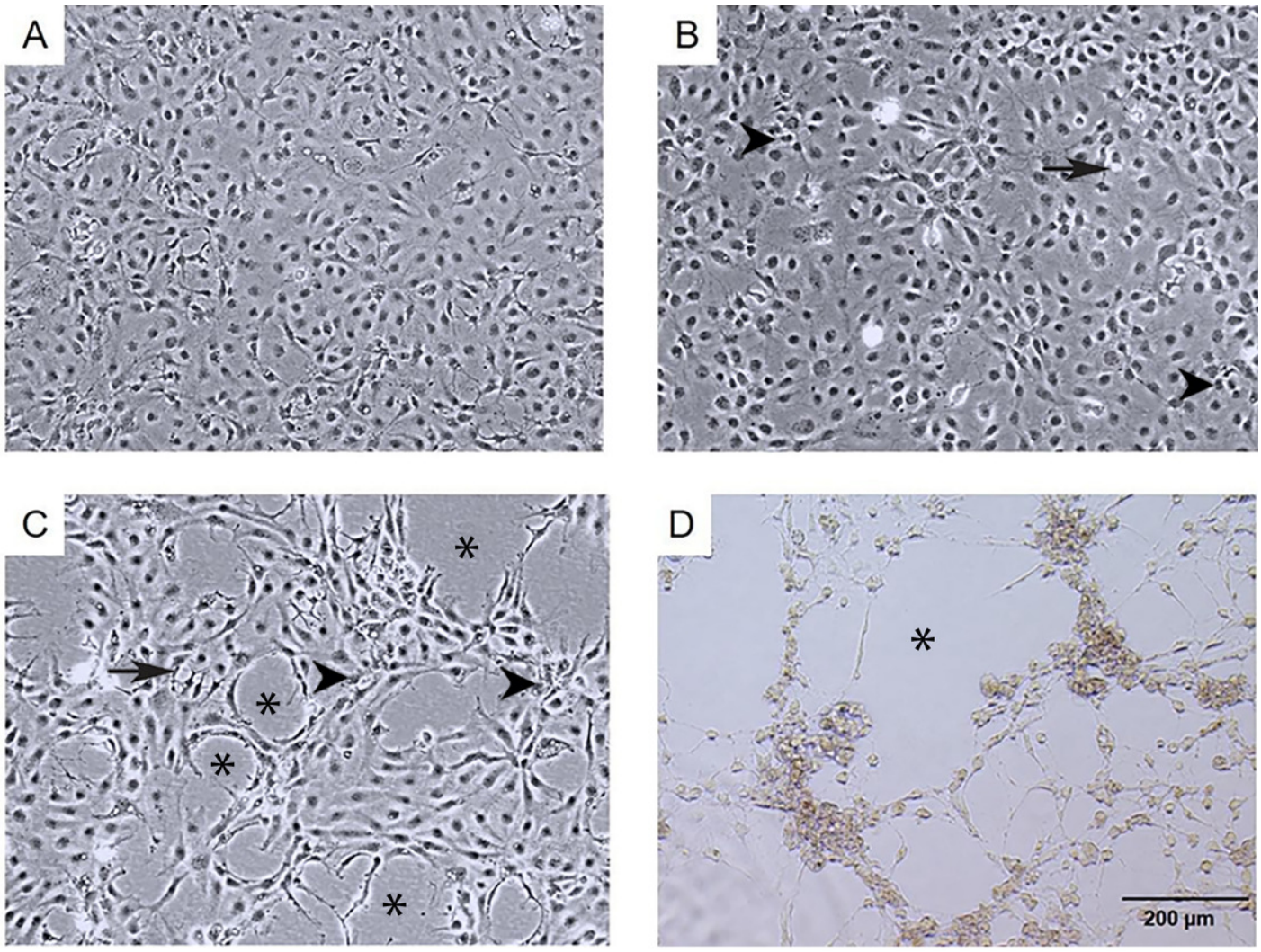

Figure 2

Representative TEM micrographs of TiLV-infected E-11 cells.

Figure 2 Representative TEM micrographs of uninfected and TiLV-infected E-11 cells at 0 dpi (1 h post-TiLV inoculation). (A) Uninfected E-11 cell with normal mitochondria (arrows), and nucleus (N). (B) TiLV-infected E-11 cell with normal nucleus (N), rough endoplasmic reticulum (rER: arrowhead), and presence of intracytoplasmic TiLV particle close to the plasma membrane (inset). (C) Uninfected E-11 cell under higher magnification showing normal mitochondria (arrow) and rER (arrowheads). (D) TiLV-infected E-11 cells under higher magnification showing normal mitochondria (arrow).

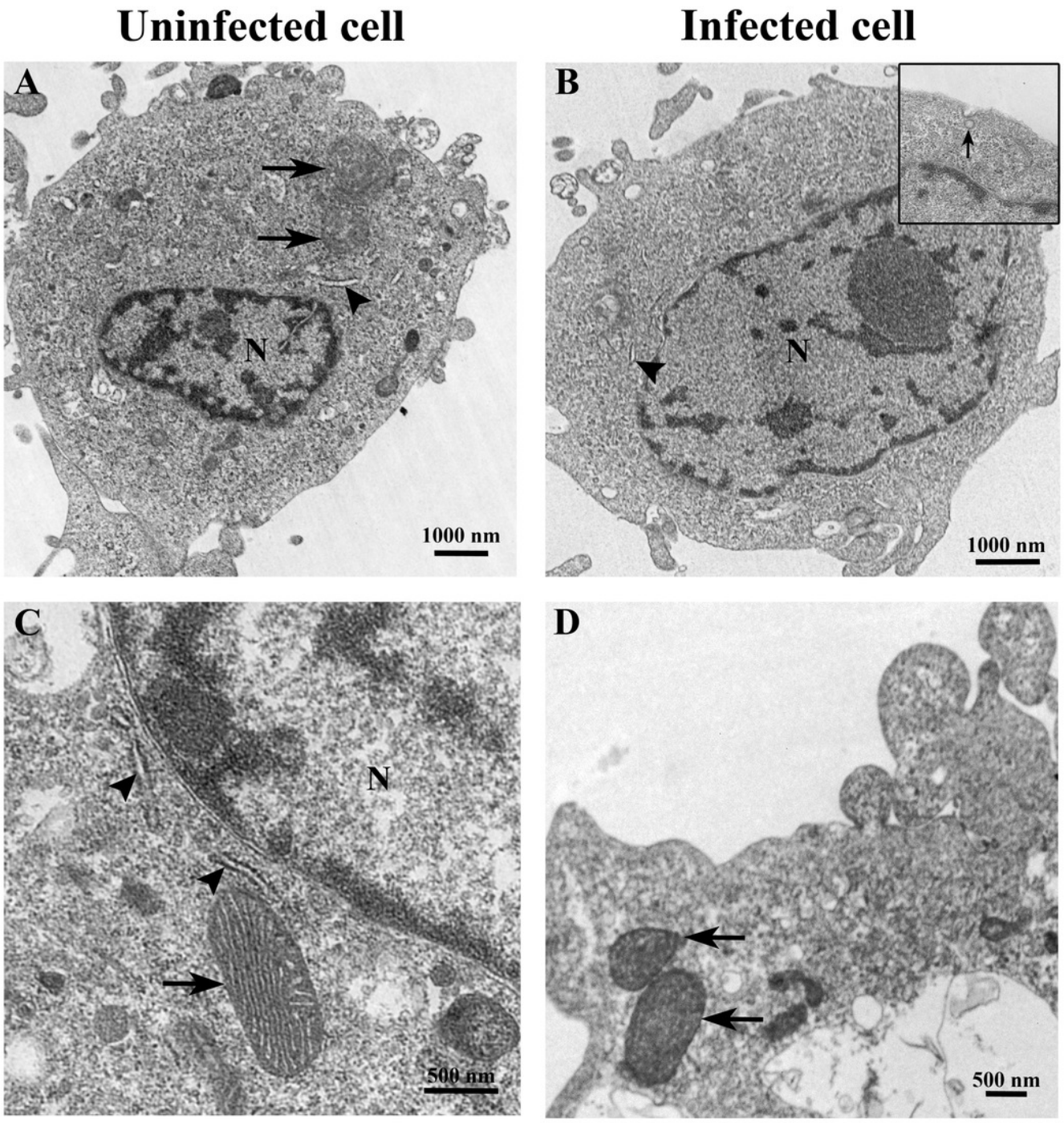
Uninfected cell
Infected cell
A
B
N
N
1000 nm
1000 nm
C
D
N
500 nm
500 nm

Figure 3

Time course analysis of ultrastructural changes of TiLV-infected E-11 cells.

Figure 3 Time course of ultrastructural changes in TiLV-infected compared to uninfected E-11 cells. (A) Uninfected cell at 1 dpi presenting a normal mitochondrion with intact cristae (white arrow) and mitochondria with partial loss of cristae (black arrows). (B) TiLV-infected cell at 1 dpi, moderate mitochondrial damage (arrowhead) with the presence of a TiLV particle close to the plasma membrane (arrow). Nuclear membrane is still intact (asterisk). (C) Uninfected cell at 3 dpi displaying normal mitochondria and some mitochondria with partial loss of cristae (arrowhead), N = nucleus. (D) TiLV-infected cell at 3 dpi, a mitochondrion without cristae (arrowhead), and abundance of TiLV particles (arrow) close to lamellar bodies (asterisk) can be seen. (E) Uninfected cell with normal mitochondrion (arrowhead) near the intact nuclear membrane (asterisk), N= nucleus. (F) TiLV-infected cell at 6 dpi presenting a group of extensive degenerated mitochondria (arrowheads) surrounding TiLV particles (arrow), N = nucleus.

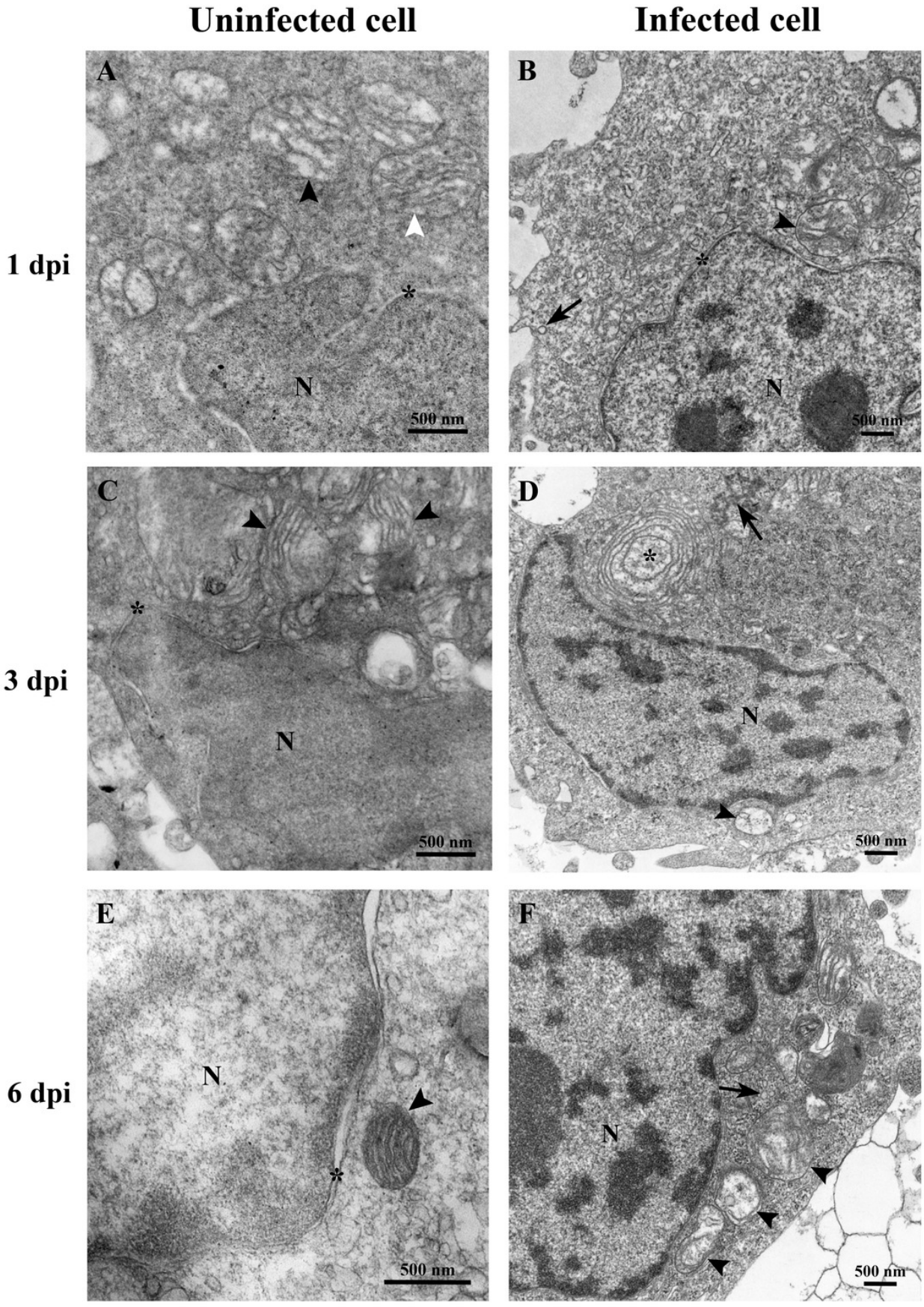
Uninfected cell
Infected cell
1 dpi
3 dpi
6 dpi
A
B
C
D
E
F
N
500 nm

Figure 4

Determination of mitochondrial damage in TiLV-infected E-11 cells.

Figure 4 Determination of mitochondrial structural and functional damage upon TiLV-infected E-11 cells at 0, 1, 3, and 6 dpi. (A) Survival of E-11 cells after TiLV infection assessed by MTT assay. (B) ATP concentration measured using CellTiter-Glo® assay (C) Mitochondrial damage in TiLV-infected cells was analyzed based on the red-to-green ratio of JC-1-stained E-11 cells. Data were quantified from three separate fields of overlay picture and shown as average values. All data were represented as the mean ± standard error of mean (S.E.M.) from three independent experiments. (D) Bright field (BF), red cells (JC-1 aggregate), green cells (JC-1 monomer), and overlay pictures of uninfected and TiLV-infected E-11 cells. Statistical significance between uninfected and TiLV-infected cells is denoted by *$p<0.05$, **$p<0.01$, and ***$p<0.001$.

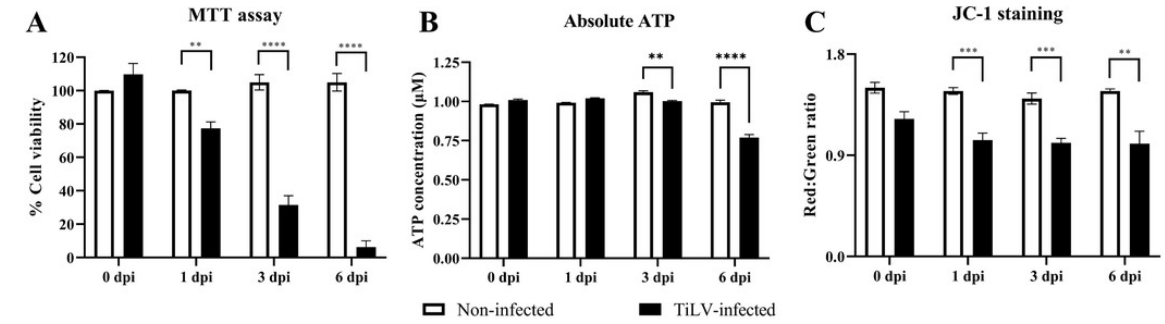
A
MTT assay
% Cell viability
0 dpi
1 dpi
3 dpi
6 dpi
B
Absolute ATP
ATP concentration (μM)
C
JC-1 staining
Red:Green ratio
Non-infected
TiLV-infected

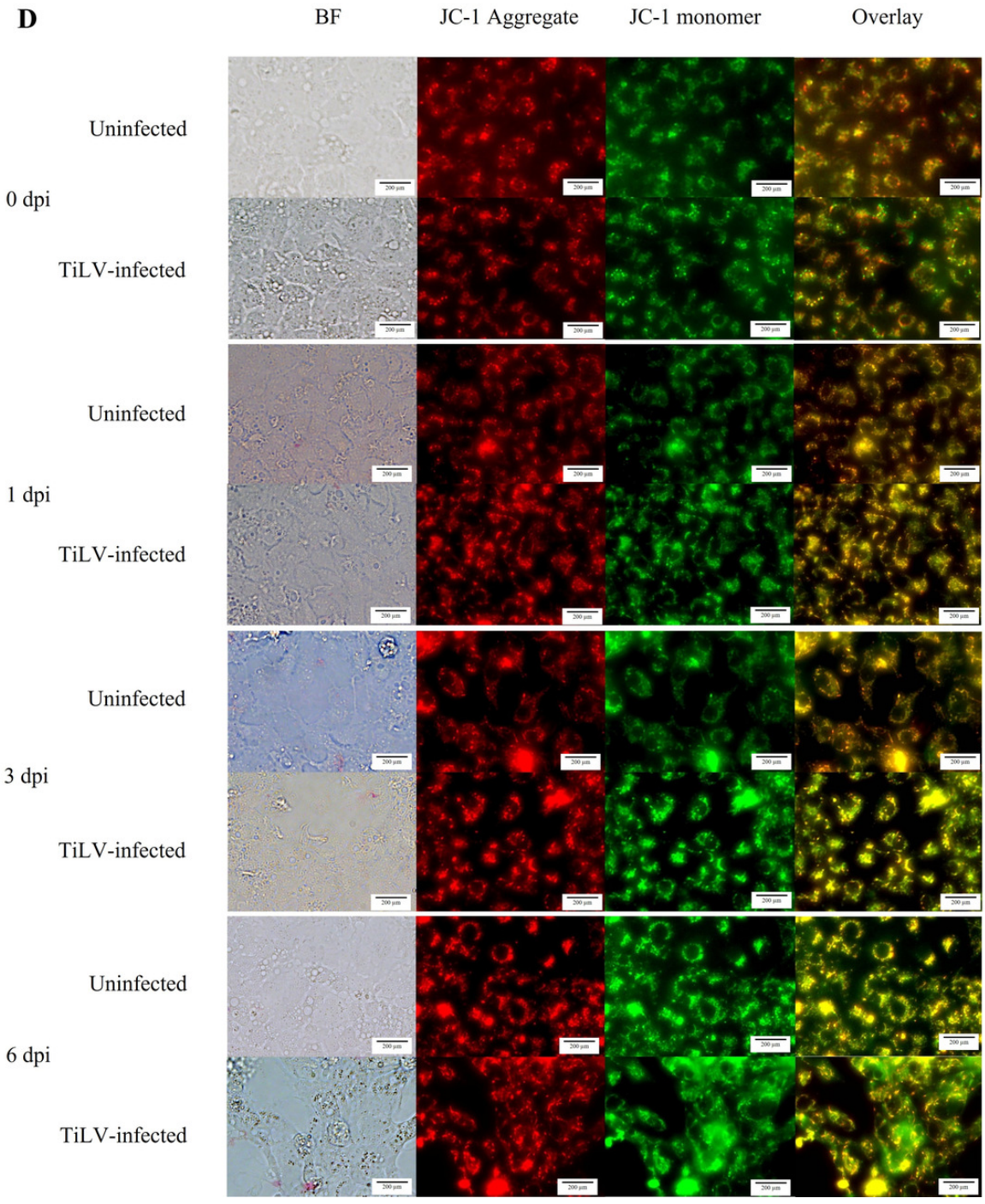
D
BF
JC-1 Aggregate
JC-1 monomer
Overlay
Uninfected
0 dpi
TiLV-infected
Uninfected
1 dpi
TiLV-infected
Uninfected
3 dpi
TiLV-infected
Uninfected
6 dpi
TiLV-infected

Figure 5

Representative images of E-11 at 1 dpi incubated with Mitotracker™ Red staining.

Representative images of E-11 at 1 dpi incubated with Mitotracker™ Red staining (A) Uninfected cells (B) TiLV-infected cells. The nuclei were stained with DAPI.